

Singular Perturbation-based Large-Signal Order Reduction of Microgrids for Stability and Accuracy Synthesis with Control

Zixiao Ma, *Member, IEEE*, Zhaoyu Wang, *Senior Member, IEEE*, Yuxuan Yuan, *Member, IEEE*, Tianqi Hong, *Member, IEEE*,

Abstract—The increasing penetration of distributed energy resources (DERs) highlights the growing importance of microgrids (MGs) in enhancing power system reliability. Employing electromagnetic transient (EMT) analysis in MGs becomes crucial for controlling the rapid transients. However, this requires an accurate but high-order model of power electronics and their underlying control loops, complexifying the stability analysis from the viewpoint of a higher control level. To overcome these challenges, this paper proposes a large-signal order reduction (LSOR) method for MGs with considerations of external control inputs and the detailed dynamics of underlying control levels based on singular perturbation theory (SPT). Specially, we innovatively proposed and strictly proved a general stability and accuracy assessment theorem that allows us to analyze the dynamic stability of a full-order nonlinear system by only leveraging our derived reduced-order model (ROM) and boundary layer model (BLM). Furthermore, this theorem furnishes a set of conditions that determine the accuracy of the developed ROM. Finally, by embedding such a theorem into the SPT, we propose a novel LSOR approach with guaranteed accuracy and stability analysis equivalence. Case studies are conducted on MG systems to show the effectiveness of the proposed approach.*

Index Terms—Microgrids, inverters, nonlinear, order reduction, singular perturbation, stability, electromagnetic transient

NOMENCLATURE

A. Abbreviations

| | |
|------|------------------------------|
| BLM | Boundary layer model |
| DER | Distributed energy resource |
| EMT | Electromagnetic transient |
| GAS | Global asymptotic stability |
| ISS | Input-to-state stability |
| LPF | Low pass filter |
| LSOR | Large-signal order reduction |
| MG | Microgrid |
| PI | Proportion-Integral |
| PLL | Phase locked loop |
| PCC | Point of common coupling |

This work was supported in part by the U.S. Department of Energy Wind Energy Technologies Office under Grant DE-EE0008956, and in part by the National Science Foundation under ECCS 1929975 and SBE 2228620. (*Corresponding author:* Zhaoyu Wang)

Z. Ma, Z. Wang and Y. Yuan are with the Department of Electrical and Computer Engineering, Iowa State University, Ames, IA, 50011 USA (E-mail: zma@iastate.edu; wzy@iastate.edu; yuanyx@iastate.edu).

T. Hong is with the School of Electrical and Computer Engineering at the University of Georgia, Athens, GA 30602, USA (e-mails: Tianqi.Hong@uga.edu).

| | |
|----------------------|--|
| QSS | Quasi-steady-state |
| RMSE | Root-mean-square error |
| ROM | Reduced-order model |
| SPT | Singular perturbation theory |
| | |
| B. Variables | |
| P, Q | Active and reactive powers |
| V_{od}, V_{oq} | dq-axis DER output voltages |
| I_{od}, I_{oq} | dq-axis DER output currents |
| V_{odf} | filtered d-axis DER output voltage |
| Φ_{PLL} | Integral of filtered d-axis DER output voltage |
| δ | Phase angle |
| ω_{PLL} | Angular frequency measured by PLL |
| Φ_P, Φ_Q | Integrals of errors between active/reactive power and power commands |
| P^*, Q^* | Active and reactive power commands |
| I_{ld}^*, I_{lq}^* | dq-axis inductor current commands |
| ω^* | Angular frequency command generated by droop controller |
| ω_n | Angular frequency setpoint |
| V_{oq}^* | DER output voltage command generated by droop controller |
| $V_{oq,n}$ | DER output voltage setpoint |
| Φ_d | Integral of error between measured angular frequency and its command |
| Φ_q | Integral of error between DER output voltage and its command |
| Γ_d, Γ_q | Integrals of errors between dq-axis inductor currents and their commands |
| V_{ld}^*, V_{lq}^* | dq-axis inductor voltage commands |
| I_{ld}, I_{lq} | dq-axis inductor currents |
| V_{bd}, V_{bq} | dq-axis bus voltages |
| \mathbf{x} | Slow state variables of the MG system |
| \mathbf{z} | Fast state variables of the MG system |
| \mathbf{u} | External control input of the MG system |
| \mathbf{y} | System output of the MG system |
| $\hat{\mathbf{x}}$ | Solution of the ROM |
| $\hat{\mathbf{y}}$ | Solution of the BLM |
| \mathbf{E}_x | Error vector between the slow states and the solution of the ROM |
| \mathbf{E}_y | Error vector between the fast states and the solution of the BLM |

C. Parameters

| | |
|---------------------------|--|
| OM_{flag} | Switch between grid-tied and islanded mode: 1-grid-tied mode; 2-islanded mode |
| ω_c | Corner frequency of LPF for instantaneous powers |
| $\omega_{\text{cPLL}i}$ | Corner frequency of LPF for DER output voltage |
| $K_{\text{P,PLL}}$ | Proportional gain of PI controller in PLL |
| $K_{\text{I,PLL}}$ | Integral gain of PI controller in PLL |
| $K_{\text{I,P}}$ | Integral gain of PI controller in power controller |
| $K_{\text{P,P}}$ | Proportional gain of PI controller in power controller |
| D_P | $P-\omega$ droop gain |
| D_Q | $Q-V$ droop gain |
| $K_{\text{I,V}}$ | Integral gain of PI controller in voltage controller |
| $K_{\text{P,V}}$ | Proportional gain of PI controller in voltage controller |
| ω_n | Nominal angular frequency |
| L_f | Inductance of LC filter |
| $K_{\text{I,C}}$ | Integral gain of PI controller in current controller |
| $K_{\text{P,C}}$ | Proportional gain of PI controller in current controller |
| R_f, R_c | Parasitic resistances of the inductors |
| C_f | Capacitance of LC filter |
| R_d | Dumping resistor of LC filter |
| ε | Perturbation coefficient |
| ε^* | Threshold of ε below which the error of ROM converges asymptotically |
| ε^{**} | Threshold of ε below which the error of ROM converges within a finite time T |
| n, m, p | Dimensions of slow/fast states and input |
| τ | Fast time scale variable defined as t/ε |
| T | Finite error convergence time if $\varepsilon < \varepsilon^{**}$ |

I. INTRODUCTION

MICROGRIDS (MGs) are localized small-scale power systems composed of interconnected loads and distributed energy resources (DERs) in low-voltage and medium-voltage distribution networks. It can be operated in grid-connected and islanded modes [1]–[6]. The high penetration of low-inertia DERs makes the dynamic response of MGs different from conventional networks dominated by synchronous machines. This low-inertia characteristic highlights the importance of dynamic modeling, stability analysis, and control studies of MGs in the electromagnetic transient (EMT) time scale [7]–[9]. To precisely capture the comprehensive transient dynamics of MGs in a hierarchical control structure, detailed dynamic models of the lower control levels such as primary and zero-control levels, and the impact of external input from higher control levels such as secondary control, need to be taken into account. However, the high-order nature of these detailed dynamics of the underlying control structures makes it intractable to analyze the stability of MGs with such a complex dynamic model [10]–[14]. In addition, an-

other critical challenge brought by considering the underlying controllers is the two-time-scale behavior of MGs due to the different evolutionary velocities of different state variables, which leads to a stiff differential equation problem [15]. In the dynamic simulation of MGs, numerically solving this stiff problem requires extremely small time steps, which results in an unmanageable computational complexity [16].

To solve the above problems, model order reduction techniques have been studied and applied to power system analyses. In [17], [18], an aggregate equivalent model was developed for the order reduction of MGs by assuming similar inverter dynamics. Kron reduction was adopted to simplify the network of MGs in [19]. In [20], the authors used a balanced truncation method for DC MGs described by a linear model with inhomogeneous initial conditions. Although these methods can effectively simplify the MG model, the time-scale separation problem aroused by the consideration of underlying control levels for EMT analysis is still not solved.

Given the inherent two-time-scale property of MGs, singular perturbation theory (SPT) is a suitable technology for this purpose. The SPT is a mathematical framework that focuses on analyzing problems with a parameter, where the solutions of the problem at a specific limiting value of the parameter exhibit distinct characteristics compared to the solutions of the general problem, resulting in a singular limit. It facilitates the separation of the system into a reduced-order model (ROM) that captures the slow states, and a boundary layer model (BLM) that represents the errors between fast and quasi-steady states. It is worth noting that the terms “slow” and “fast” refer to the transient evolutionary velocity of states in this context. Unlike conventional model reduction methods that simply neglect certain state variables, SPT preserves the characteristics of fast dynamics by integrating them into the “slow” states, as advocated by [21]. Additionally, SPT has the advantage of converting the original stiff problem into a non-stiff problem, resulting in improved computational efficiency. Due to the above advantages, the SPT has been widely used in power system studies. The transient stability of type-3 wind turbines is investigated in [22] by applying the SPT and Lyapunov methods and taking into account the dynamics of phase-locked loop (PLL) and current control. In [23], a model-order reduction and dynamic aggregation strategy are proposed for grid-forming inverter-based power networks. More reduced-order models for grid-forming virtual-oscillator-controlled inverters with nested current and voltage-control loops, and current-limiting action for overcurrent protection by using the SPT are outlined in [24]. In [25], a linear active disturbance rejection control scheme for two-mass systems is developed based on the SPT. In the context of the MG order reduction problem, a spatiotemporal model reduction method of MGs using SPT and Kron reduction was proposed in [26], nonetheless, the method is not generic enough. In [27], [28], a linear SPT was applied to small-signal models of MGs. A small-signal ROM considering coupling dynamics is developed for autonomous wind-solar multi-MGs based on the SPT in [29]. However, since the above studies use the small-signal model, the results only hold in the neighborhood of a stable equilibrium point.

The above studies focus on the development of the reduced-order MG modeling, whereas the stability assessment based on the derived ROM is not included. To fill this gap, the system order is reduced to simplify the stability analysis by neglecting the underlying voltage controller in [30] at the expense of losing fast dynamics. In [31], the nonlinear Lyapunov stability of DC/AC inverters with different ROMs was studied. A method for simplifying the stability assessment was developed and applied to an islanded MG with droop control by using inverter angles in [32]. Nevertheless, it was demonstrated that such a simplification process could affect the accuracy of ROMs in [33]–[35]. Moreover, to our best knowledge, the existing studies *do not consider the impact of external inputs* such as power commands and voltage frequency references on MG stability analysis. A typical way is to consider the unforced system by neglecting the inputs to study the internal stability. However, even though the unforced system is stable, a continuous input signal can render the system unstable. In [36], a stability assessment criterion that used the input-to-state stability (ISS) of ROM and global asymptotic stability (GAS) of BLM was proposed to analyze the total stability of the original system. This method is generic for arbitrary singular perturbed systems under certain conditions, nevertheless, the convergence of the error between reduced and original models is not theoretically analyzed, which hinders the accuracy evaluation of ROMs. This work is further extended in [37], where the stability and accuracy issues are simultaneously proved, however, the effect of external inputs is still not analyzed.

To overcome the above challenges, this paper proposes a novel large-signal order reduction (LSOR) strategy for inverter-based MGs with detailed dynamics of the underlying control levels in the EMT time scale. Firstly, a general theorem for analyzing the dynamic stability of the full-order model by only alternatively assessing the stability of its derived ROM and BLM is proposed. A key point is that we consider ISS to quantify the system's response to external inputs and unify internal and external stability. In particular, by assuming the ROM to be ISS, the unforced ROM to be exponentially stable, and BLM to be uniformly GAS, one can prove that the original system is totally ISS. Then, we develop the conditions that guarantee the accuracy of ROMs for both slow and fast dynamics. Finally, by embedding the proposed stability and accuracy assessment theorem into the large-signal SPT, an improved LSOR algorithm is proposed for MGs. Strict mathematical proof is provided to illustrate that the proposed order reduction technique is generic for arbitrary dynamic systems. The main contributions can be summarized as follows:

- We propose a general theorem that allows us to assess the large-signal stability of MGs with detailed dynamics of underlying controllers in the EMT time scale by only analyzing their ROMs and BLMs.
- A set of accuracy criteria is developed, under which the error between the reduced and original models is bounded and converges as the perturbation coefficients decrease.
- The impact of external control input from the higher

control level on the above stability and accuracy analyses is studied with strict mathematical proof.

- The stability and accuracy assessment synthesis is embedded into the LSOR method to improve the model accuracy via a feedback mechanism, which automatically tunes the bounds of perturbation coefficients as an index for identifying the slow and fast dynamics.

The rest of the paper is organized as follows. Section II describes the large-signal mathematical model of the studied MG system. Section III introduces the general singular perturbation theory and proposes our stability and accuracy assessment theory. Section IV gives the simulation validation of the proposed method. Section V concludes the paper.

II. LARGE-SIGNAL MODELING OF INVERTER-BASED MGs

This section introduces a nonlinear model of the studied MG system with detailed primary and zero-control levels. Depending on the research objectives, control strategies, and operation modes, MGs may have different models. According to [27], the transient response velocity of line dynamics is much faster than the slow ones in DERs due to the small line impedance. Moreover, the state equations are fully decoupled between DERs and lines. As a result, the line dynamics can be neglected. Therefore, this section focuses on the modeling of DERs, which are the main dynamic components in an inverter-based MG.

A general control diagram of DERs is shown in Fig. 1. The model can switch between two subsystems according to the MG operation modes. In grid-tied mode, OM_{flag} switches to 1, then the voltage source inverter is controlled by the power controller and current controller to follow the power command (P^*, Q^*) . The MG bus voltage and system frequency are maintained by the main grid. In islanded mode, OM_{flag} is set to 0, and the MG voltage and frequency are regulated by the DERs using droop controllers. According to Fig. 1, the mathematical model can be derived for each component where $i = 1, \dots, N$ denotes the index of N DERs in the MG.

A. Average Power Calculation

The generated active and reactive power can be calculated using the transformed output voltage v_{odq} and current i_{odq} . Using a low-pass filter (LPF) with the corner frequency ω_c , we can obtain the filtered instantaneous powers as follows,

$$\dot{P}_i = -P_i\omega_{ci} + 1.5\omega_{ci}(V_{odi}I_{odi} + V_{oqi}I_{oqi}), \quad (1a)$$

$$\dot{Q}_i = -Q_i\omega_{ci} + 1.5\omega_{ci}(V_{oqi}I_{odi} - V_{odi}I_{oqi}). \quad (1b)$$

B. Phase Lock Loop

The model of PLL is the same as that established in [27] as follows,

$$\dot{V}_{odfi} = \omega_{cPLLi}V_{odi} - \omega_{cPLLi}V_{odfi}, \quad (2a)$$

$$\dot{\Phi}_{PLLi} = -V_{odfi}. \quad (2b)$$

In grid-tied mode, the inverter output phase is synchronized to the main grid using PLL, therefore the derivative of phase angle δ_i is set to ω_{PLLi} :

$$\dot{\delta}_i = \omega_{PLLi} = 377 - K_{P,PLLi}V_{odfi} + K_{I,PLLi}\bar{\Phi}_{PLLi}. \quad (3)$$

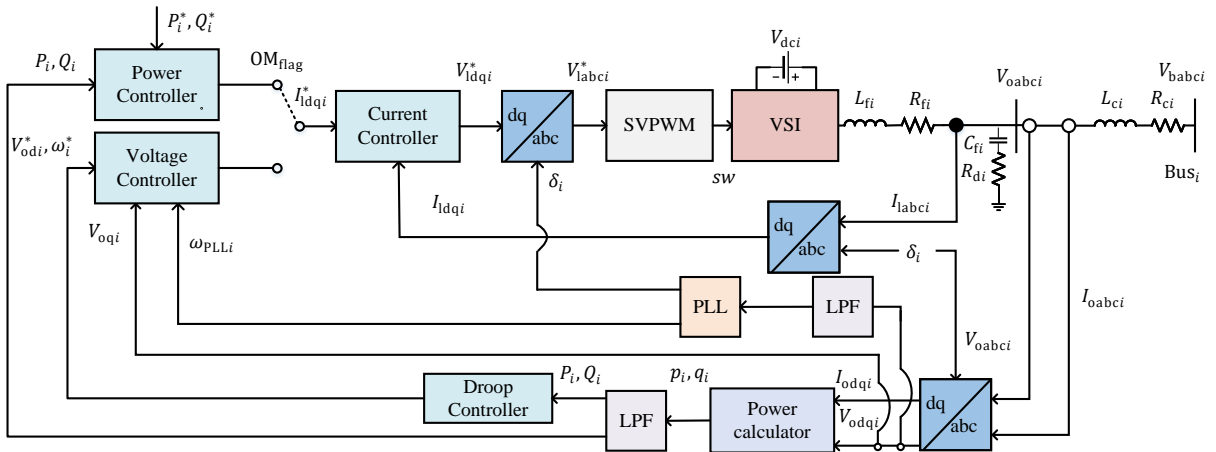


Fig. 1. The block diagram of voltage-sourced inverter-based DER with underlying control loops.

In islanded mode, the phase angle of the first inverter can be arbitrarily set as the reference for the other inverters:

$$\dot{\delta}_i = \omega_{\text{PLL}1} - \omega_{\text{PLL}i}. \quad (4)$$

C. Power Controllers

In grid-tied mode, the output power of DER is regulated by the power controller using the PI control method. The input references are the commanded real and reactive powers:

$$\dot{\Phi}_{Pi} = P_i - P_i^*, \quad (5a)$$

$$I_{lqi}^* = K_{I,Pi}\dot{\Phi}_{Pi} + K_{P,Pi}\dot{\Phi}_{Qi}, \quad (5b)$$

$$\dot{\Phi}_{Qi} = Q_i - Q_i^*, \quad (5c)$$

$$I_{ldi}^* = K_{I,Pi}\dot{\Phi}_{Qi} + K_{P,Pi}\dot{\Phi}_{Qi}. \quad (5d)$$

D. Voltage Controllers and Droop Controllers

In islanded mode, a DER has no reference inputs from the main grid. Therefore, it must generate its own voltage and frequency references using droop controllers as follows,

$$\omega_i^* = \omega_{ni} - D_{Pi}P_i, \quad (6a)$$

$$V_{oqi}^* = V_{oq,ni} - D_{Qi}Q_i. \quad (6b)$$

These references will be used as the set points for voltage controllers. Two PI controllers are adopted for the voltage controllers as follows,

$$\dot{\Phi}_{di} = \omega_{\text{PLL}i} - \omega_i^*, \quad (7a)$$

$$I_{ldi}^* = K_{I,Vi}\dot{\Phi}_{di} + K_{P,Vi}\dot{\Phi}_{di}, \quad (7b)$$

$$\dot{\Phi}_{qi} = V_{oqi}^* - V_{oqi}, \quad (7c)$$

$$I_{lqi}^* = K_{I,Vi}\dot{\Phi}_{qi} + K_{P,Vi}\dot{\Phi}_{qi}. \quad (7d)$$

E. Current Controllers

The PI controllers are adopted for current controllers. They generate the commanded voltage reference V_{ldqi}^* according to

the error between the inductor currents reference I_{ldqi}^* and its feedback measurements I_{ldqi} :

$$\dot{\Gamma}_{di} = I_{ldi}^* - I_{ldi}, \quad (8a)$$

$$V_{ldi}^* = -\omega_{ni}L_{fi}I_{lqi} + K_{I,Ci}\Gamma_{di} + K_{P,Ci}\dot{\Gamma}_{di}, \quad (8b)$$

$$\dot{\Gamma}_{qi} = I_{lqi}^* - I_{lqi}, \quad (8c)$$

$$V_{lqi}^* = -\omega_{ni}L_{fi}I_{ldi} + K_{I,Ci}\Gamma_{qi} + K_{P,Ci}\dot{\Gamma}_{qi}. \quad (8d)$$

F. LC Filters and Coupling Inductors

The dynamical models of LC filters and coupling inductors are as follows,

$$\dot{I}_{ldi} = (-R_{fi}I_{ldi} + V_{ldi} - V_{odi}) / L_{fi} + \omega_{ni}I_{lqi}, \quad (9a)$$

$$\dot{I}_{lqi} = (-R_{fi}I_{lqi} + V_{lqi} - V_{oqi}) / L_{fi} - \omega_{ni}I_{ldi}, \quad (9b)$$

$$\dot{I}_{odi} = (-R_{ci}I_{odi} + V_{odi} - V_{bdi}) / L_{ci} + \omega_{ni}I_{oqi}, \quad (9c)$$

$$\dot{I}_{oqi} = (-R_{ci}I_{oqi} + V_{oqi} - V_{bqi}) / L_{ci} - \omega_{ni}I_{odi}, \quad (9d)$$

$$\dot{V}_{odi} = (I_{ldi} - I_{odi}) / C_{fi} + \omega_{ni}V_{oqi} + R_{di}(\dot{I}_{ldi} - \dot{I}_{odi}), \quad (9e)$$

$$\dot{V}_{oqi} = (I_{lqi} - I_{oqi}) / C_{fi} - \omega_{ni}V_{odi} + R_{di}(\dot{I}_{lqi} - \dot{I}_{oqi}). \quad (9f)$$

In conclusion, when the MG system is operating in grid-tied mode, the mathematical model can be represented by equations (1)-(3), (5) and (8)-(9). In islanded mode, the MG model can be represented by equations (1)-(2), (4) and (6)-(9).

III. IMPROVED LSOR BY EMBEDDING STABILITY AND ACCURACY ASSESSMENT THEOREM

In this section, we propose an improved LSOR method together with stability and accuracy assessment synthesis. Firstly, we briefly present the SPT-based LSOR approach. Then a novel large-signal stability and accuracy assessment theorem with consideration of external control input is proposed. Finally, we improve the LSOR algorithm by embedding the stability and accuracy assessment theorem, so that it can guarantee the accuracy of derived ROM and efficiently evaluate the stability of original models. The proposed LSOR strategy is essentially generic and is suitable for the above MG model introduced in Section II.

A. LSOR Approach using the SPT for MGs

Due to the two-time-scale property, the dynamics of MGs can be classified as slow and fast dynamics according to the transient velocities. Based on this phenomenon, here we first rewrite the mathematical model introduced in Section II as the general singular perturbed form (10). Then, the detailed algorithm, theoretical supports, and case studies illustrating the identification of slow and fast will be proposed in the later sections.

$$\dot{\mathbf{x}}(t) = \mathbf{f}(\mathbf{x}(t), \mathbf{z}(t), \mathbf{u}(t), \varepsilon), \quad (10a)$$

$$\varepsilon \dot{\mathbf{z}}(t) = \mathbf{g}(\mathbf{x}(t), \mathbf{z}(t), \mathbf{u}(t), \varepsilon), \quad (10b)$$

where all the state variables in (1)-(9) are collected in the vector $[\mathbf{x}^\top \mathbf{z}^\top]^\top = [P_i Q_i V_{\text{odfi}} \Phi_{\text{PLL}_i} \delta_i \Phi_{\text{Pi}} \Phi_{\text{Qi}} \Gamma_{\text{di}} \Gamma_{\text{qi}} I_{\text{lodi}} I_{\text{lqi}} V_{\text{odi}} V_{\text{oqi}} I_{\text{odi}} I_{\text{oqi}}]^\top (i = 1, \dots, N)$ in grid-tied mode or $[\mathbf{x}^\top \mathbf{z}^\top]^\top = [P_i Q_i \Phi_{\text{PLL}_i} V_{\text{odfi}} \delta_i \Phi_{\text{di}} \Phi_{\text{qi}} \Gamma_{\text{di}} \Gamma_{\text{qi}} I_{\text{lodi}} I_{\text{lqi}} V_{\text{odi}} V_{\text{oqi}} I_{\text{odi}} I_{\text{oqi}}]^\top (i = 1, \dots, N)$ in islanded mode, respectively; $\dot{\mathbf{x}} \in \mathbb{R}^n$ and $\dot{\mathbf{z}} \in \mathbb{R}^m$ denote the derivatives of slow and fast states, respectively; the external control input is denoted as $\mathbf{u} = [P_i^* Q_i^*]^\top$ in grid-tied mode or $\mathbf{u} = [\omega_{ni} V_{\text{oq},ni}]^\top$ in islanded mode, respectively; ε denotes the small parameters in MGs such as capacitances and inductances named as perturbation coefficient and its identification method will be proposed in the later sections; \mathbf{f} and \mathbf{g} are locally Lipschitz functions on their arguments. For simplicity, we neglect the notation of time-dependency (t) in the rest of this paper.

The two-time-scale characteristic of MGs motivates the adoption of SPT. The main idea of SPT is to *freeze* the fast dynamics and degenerate them into static equations. Thus, the ROM can be obtained by substituting the solutions of the static equations into the slow dynamic equations. Since ε is small, the fast transient velocity $\dot{\mathbf{z}} = \mathbf{g}/\varepsilon$ can be much larger than the slow dynamics $\dot{\mathbf{x}}$. To solve this two-time-scale problem, we can set $\varepsilon = 0$, then equation (10b) degenerates to the following algebraic equation,

$$0 = \mathbf{g}(\mathbf{x}, \mathbf{z}, \mathbf{u}, 0). \quad (11)$$

If equation (11) has at least one isolated real root and satisfies the implicit function theory, then for each argument, we have the following closed-form solution,

$$\mathbf{z} = \mathbf{h}(\mathbf{x}, \mathbf{u}). \quad (12)$$

Substitute equation (12) into equation (10a) and let $\varepsilon = 0$, we have a quasi-steady-state (QSS) model,

$$\dot{\mathbf{x}} = \mathbf{f}(\mathbf{x}, \mathbf{h}(\mathbf{x}, \mathbf{u}), \mathbf{u}, 0). \quad (13)$$

Note that the order of the QSS system (13) drops from $n+m$ to n . The inherent two-time-scale property can be described by introducing the BLM. Define a fast time scale variable $\tau = t/\varepsilon$, and a new coordinate $\mathbf{y} = \mathbf{z} - \mathbf{h}(\mathbf{x}, \mathbf{u})$. In this new coordinate, equation (10b) is rewritten as

$$\begin{aligned} \frac{d\mathbf{y}}{d\tau} &= \mathbf{g}(\mathbf{x}, \mathbf{y} + \mathbf{h}(\mathbf{x}, \mathbf{u}), \mathbf{u}, \varepsilon) \\ &\quad - \varepsilon \left[\frac{\partial \mathbf{h}}{\partial \mathbf{x}} \mathbf{f}(\mathbf{x}, \mathbf{y} + \mathbf{h}(\mathbf{x}, \mathbf{u}), \mathbf{u}, \varepsilon) + \frac{\partial \mathbf{h}}{\partial \mathbf{u}} \dot{\mathbf{u}} \right]. \end{aligned} \quad (14)$$

Let $\varepsilon = 0$, we obtain the BLM as follows,

$$\frac{dy}{d\tau} = \mathbf{g}(\mathbf{x}, \mathbf{y} + \mathbf{h}(\mathbf{x}, \mathbf{u}), \mathbf{u}, 0). \quad (15)$$

B. Stability and Accuracy Assessment Theorem

In this subsection, we propose a criterion to assess the stability of the original system and the accuracy of ROM and BLM. We first introduce a few technical definitions and assumptions below.

Definition 1: Class \mathcal{K} function $\alpha : [0, t) \rightarrow [0, \infty)$ is a continuous strictly increasing function with $\alpha(0) = 0$. Further, if $t = \infty$ and $\lim_{r \rightarrow \infty} \alpha(r) = \infty$, then α is said to belong to class \mathcal{K}_∞ function.

Definition 2: Class \mathcal{KL} function $\beta : [0, t) \times [0, \infty) \rightarrow [0, \infty)$ is a continuous function satisfying: for each fixed s , the function $\beta(r, s)$ belongs to class \mathcal{K} ; for each fixed r , the function $\beta(r, s)$ is decreasing with respect to s and $\beta(r, s) \rightarrow 0$ for $s \rightarrow \infty$.

Considering the impact of external inputs on the stability of MGs, we define the ISS as follows.

Definition 3 (ISS): Consider such a nonlinear system

$$\dot{\mathbf{x}} = \tilde{\mathbf{f}}(\mathbf{x}, v_1, v_2) \quad (16)$$

where $\mathbf{x} \in \mathbb{R}^n$ is the state vector, $v_1 \in \mathbb{R}^m$, $v_2 \in \mathbb{R}^p$ are input vectors, and $\tilde{\mathbf{f}}$ is locally Lipschitz on $\mathbb{R}^n \times \mathbb{R}^m \times \mathbb{R}^p$. The system (16) is ISS with Lyapunov gains α_{v_1} and α_{v_2} of class \mathcal{K} , if there exists a class \mathcal{KL} function β such that for $\mathbf{x}(0) \in \mathbb{R}^n$ and bounded inputs v_1, v_2 , the solution of (16) exists and satisfies

$$\|\mathbf{x}(t)\| \leq \beta(\|\mathbf{x}(0)\|, t) + \alpha_{v_1}(\|v_1\|) + \alpha_{v_2}(\|v_2\|). \quad (17)$$

The above definition indicates that an MG system is ISS when all the trajectories are bounded by some functions of the input magnitudes. Then we give the following three assumptions which are the sufficient conditions for the theorem.

Assumption 1 (Growth conditions): The functions \mathbf{f} , \mathbf{g} , and their first partial derivatives are continuous and bounded with respect to $(\mathbf{x}, \mathbf{z}, \mathbf{u}, \varepsilon)$; \mathbf{h} and its first partial derivatives $\partial \mathbf{h} / \partial \mathbf{x}$, $\partial \mathbf{h} / \partial \mathbf{u}$ is locally Lipschitz; and the Jacobian $\partial \mathbf{g} / \partial \mathbf{z}$ has bounded first partial derivatives with respect to its arguments.

Assumption 2 (Stability of ROM): The ROM (13) is ISS with Lyapunov gain $\hat{\alpha}_x$, and its unforced system has an exponentially stable equilibrium at the origin.

Assumption 3 (Stability of BLM): The origin of the BLM (15) is a GAS equilibrium, uniformly in $\mathbf{x} \in \mathbb{R}^n$, $\mathbf{u} \in \mathbb{R}^p$.

Remark 1: The conditions in Assumption 1 are commonly satisfied for most MGs [34]. Inspired by [36], we propose the stability and accuracy assessment of MGs as the following theorem. Note that the conditions, results and proof of our theorem and [36] are different. In [36], only the stability of the original system is proved, nonetheless, the accuracy of the ROM and BLM is not analyzed, which is of vital importance to make sure that the derived reduced-order model is correct. However, the addition of accuracy analysis arouses new challenges in the proof which cannot be solved by directly using [36]. Therefore, we add a constraint condition on the

transient speed in Assumption 2 and propose a new proving method for our theorem.

Theorem 1: If the MGs system (10), its ROM (13) and the BLM (15) satisfy the Assumptions 1-3, then for each pair of (μ, ξ) , there exists a positive constant ε^* , such that for all $t \in [0, \infty)$, $\max \{\|\mathbf{x}(0)\|, \|\mathbf{y}(0)\|, \|\mathbf{u}\|, \|\dot{\mathbf{u}}\|\} \leq \mu$, and $\varepsilon \in (0, \varepsilon^*]$ the errors between the solutions of the original MGs system (10) and its ROM (13) and BLM (15) satisfy

$$\|\mathbf{x}(t, \varepsilon) - \hat{\mathbf{x}}(t)\| = O(\varepsilon), \quad (18)$$

$$\|\mathbf{z}(t, \varepsilon) - \mathbf{h}(\hat{\mathbf{x}}(t), \mathbf{u}(t)) - \hat{\mathbf{y}}(\tau)\| = O(\varepsilon), \quad (19)$$

where $\hat{\mathbf{x}}(t)$ and $\hat{\mathbf{y}}(\tau)$ are the solutions of ROM (13) and BLM (15), respectively. $\|\mathbf{x} - \hat{\mathbf{x}}\| = O(\varepsilon)$ means that $\|\mathbf{x} - \hat{\mathbf{x}}\| \leq k \|\varepsilon\|$ for some positive constant k . Furthermore, for any given $T > 0$, there exists a positive constant $\varepsilon^{**} \leq \varepsilon^*$ such that for $t \in [T, \infty)$ and $\varepsilon < \varepsilon^{**}$, it follows uniformly that

$$\|\mathbf{z}(t, \varepsilon) - \mathbf{h}(\hat{\mathbf{x}}(t), \mathbf{u}(t))\| = O(\varepsilon). \quad (20)$$

Moreover, there exist class \mathcal{KL} functions β_x, β_y , a Lyapunov gain α_x of class \mathcal{K} and positive constants ξ , such that the solutions of the original MGs system (10a) and (14) exist and satisfy

$$\|\mathbf{x}(t, \varepsilon)\| \leq \beta_x (\|\mathbf{x}(0)\|, t) + \alpha_x (\|\mathbf{u}\|) + \xi, \quad (21)$$

$$\|\mathbf{y}(t, \varepsilon)\| \leq \beta_y (\|\mathbf{y}(0)\|, \tau) + \xi. \quad (22)$$

Remark 2: Theorem 1 indicates large-signal stability by observing that μ can be arbitrarily large. This is more comprehensive than the small-signal stability studied in [27]. Moreover, the errors between the solutions of reduced and original MGs should be small and bounded to guarantee accuracy. (18) and (19) show that for sufficiently small ε , these errors tend to be zero. Equation (20) means that for small enough ε , the solution $\hat{\mathbf{y}}$ of the BLM decays to zero exponentially fast in time T , so that the fast solutions can be estimated by only QSS solutions $\mathbf{h}(t, \bar{\mathbf{x}}(t))$ after time T .

Remark 3: According to the theorem, if the ROM is ISS and BLM is GAS, then the original system is stable as shown in (21) and (22). Moreover, in real physical systems, one challenge of SPT is how to identify the slow and fast dynamic states. A commonly used approach is the knowledge discover-based method that relies on expert knowledge for specific domains. For example, in MGs, some small parasitic parameters such as capacitances, inductances, and small time constants, can be selected as the perturbation coefficients ε . The states with respect to these small ε are identified as fast states. This conventional empirical identification method falls short of efficiency and accuracy. Therefore, we propose a more efficient and accurate method to identify the slow/fast dynamics by finding the bound of ε in the following proof.

Proof: The proof of the theorem is conducted in three steps. First, we prove the GAS of \mathbf{y} (22). This result will then be used in proving the accuracy of ROM and BLM (18)-(20). Finally, we provide the proof of ISS of \mathbf{x} (21).

Using the converse theorem and Assumption 3, there exists a smooth function $V_1(\mathbf{x}, \mathbf{y}, \mathbf{u}) : \mathbb{R}^n \times \mathbb{R}^m \times \mathbb{R}^p \rightarrow \mathbb{R}_{\geq 0}$, and three class \mathcal{K}_∞ functions α_1, α_2 and α_3 , such that

$$\alpha_1 (\|\mathbf{y}\|) \leq V_1(\mathbf{x}, \mathbf{y}, \mathbf{u}) \leq \alpha_2 (\|\mathbf{y}\|), \quad (23)$$

$$\frac{\partial V_1}{\partial \mathbf{y}} g(\mathbf{x}, \mathbf{y} + h(\mathbf{x}, \mathbf{u}), \mathbf{u}, 0) \leq -\alpha_3 (\|\mathbf{y}\|). \quad (24)$$

Using Lemma 1 and Lemma 2 in [36] together with (23) and (24), it can be verified that there exists a class \mathcal{K} function α_y , a class \mathcal{KL} function β_y and a continuous nonincreasing function $\gamma_y : \mathbb{R}_{\geq 0} \rightarrow \mathbb{R}_{\geq 0}$, such that for essentially bounded inputs and $\varepsilon \leq \gamma_y (\max \{\|\mathbf{x}\|, \|\mathbf{y}(0)\|, \|\mathbf{u}\|, \|\dot{\mathbf{u}}\|\})$, the solution of (14) exists for all $t \geq 0$ and satisfies

$$\|\mathbf{y}(t, \varepsilon)\| \leq \beta_y (\|\mathbf{y}(0)\|, \tau) + \alpha_y (\varepsilon). \quad (25)$$

Note that at this step we do not know the boundedness of \mathbf{x} . To use the inequality (25), we apply the causality and signal truncations. Define a positive constant $\tilde{\mu}$ satisfying $\tilde{\mu} > \beta_x(\mu, 0) + \alpha_x(\mu) + \xi$. It can be verified that $\mu < \tilde{\mu}$. Considering the continuity for a given initial condition, we can define $T > 0$ as the upper bound of $[0, T)$ within which $\|\mathbf{x}\| \leq \tilde{\mu}$. Since γ_y is nonincreasing, it follows that

$$\gamma_y(\tilde{\mu}) < \gamma_y(\mu) \leq \gamma_y(\max \{\|\mathbf{x}(0)\|, \|\mathbf{y}(0)\|, \|\mathbf{u}\|, \|\dot{\mathbf{u}}\|\}), \quad (26)$$

$$\gamma_y(\tilde{\mu}) \leq \gamma_y(\|\mathbf{x}\|). \quad (27)$$

For $\varepsilon \leq \varepsilon_1 := \gamma_y(\tilde{\mu})$, (26) and (27) yield that $\varepsilon \leq \gamma_y(\max \{\|\mathbf{x}\|, \|\mathbf{y}(0)\|, \|\mathbf{u}\|, \|\dot{\mathbf{u}}\|\})$ holds for all $t \in [0, T)$. However, from the definition of $\tilde{\mu}$, there must exist a positive constant η , such that $\|\mathbf{x}\| < \tilde{\mu}$ for all $t \in [0, T + \eta)$. This contradicts that T is maximal, so $T = \infty$. Therefore, there exists an ε_2 satisfying $\alpha_y(\varepsilon_2) = \xi$, such that (22) holds for all $t \geq 0$, and $\varepsilon \leq \min\{\varepsilon_1, \varepsilon_2\}$.

Then, we prove the second step about the accuracy of the ROM (18)-(20). Define the error between solutions of reduced and original slow dynamics as $\mathbf{E}_x = \mathbf{x} - \hat{\mathbf{x}}$. When $\varepsilon = 0$, $\mathbf{y} = \mathbf{z} - \mathbf{h}(\mathbf{x}, \mathbf{u}) = 0$. Then, we have

$$\dot{\mathbf{E}}_x = \mathbf{f}(\mathbf{E}_x, 0, \mathbf{u}, 0) + \Delta \mathbf{f}, \quad (28)$$

where $\Delta \mathbf{f} = [\mathbf{f}(\hat{\mathbf{x}} + \mathbf{E}_x, 0, \mathbf{u}, 0) - \mathbf{f}(\hat{\mathbf{x}}, 0, \mathbf{u}, 0) - \mathbf{f}(\mathbf{E}_x, 0, \mathbf{u}, 0)] + \mathbf{f}(\mathbf{x}, \mathbf{y}, \mathbf{u}, \varepsilon) - \mathbf{f}(\mathbf{x}, 0, \mathbf{u}, 0)$. According to Assumption 1, it follows that

$$\begin{aligned} \|\Delta \mathbf{f}\| &\leq \ell_1 \|\mathbf{E}_x\|^2 + \ell_2 \|\mathbf{E}_x\| \|\hat{\mathbf{x}}\| \\ &\quad + \ell_3 \beta_y (\|\mathbf{y}(0)\|, \tau) + \ell_3 \xi + \ell_4 \varepsilon, \end{aligned} \quad (29)$$

for some positive constants $\ell_1, \ell_2, \ell_3, \ell_4$. The last term in system (28) can be viewed as a perturbation of

$$\dot{\mathbf{E}}_x = \mathbf{f}(\mathbf{E}_x, 0, \mathbf{u}, 0). \quad (30)$$

Since the origin of the system (30) is exponentially stable with $\mathbf{u} = 0$, using the converse theorem, there exist a Ly-

punov function $V_2(\mathbf{E}_x)$, and positive constants c_1, c_2, c_3, c_4 , for which it follows that

$$c_1 \|\mathbf{E}_x\|^2 \leq V_2(\mathbf{E}_x) \leq c_2 \|\mathbf{E}_x\|^2, \quad (31)$$

$$\frac{\partial V_2}{\partial \mathbf{E}_x} \mathbf{f}(\mathbf{E}_x, 0, \mathbf{u}, 0) \leq -c_3 \|\mathbf{E}_x\|^2, \quad (32)$$

$$\left\| \frac{\partial V_2}{\partial \mathbf{E}_x} \right\| \leq c_4 \|\mathbf{E}_x\|. \quad (33)$$

Using (22), (29) and (31)-(33), the Lyapunov function of (30) along the trajectory of (28) satisfies

$$\begin{aligned} \dot{V}_2 &= \frac{\partial V_2}{\partial \mathbf{E}_x} \mathbf{f}(\mathbf{E}_x, 0, \mathbf{u}, 0) + \frac{\partial V_2}{\partial \mathbf{E}_x} \Delta \mathbf{f} \\ &\leq -c_3 \|\mathbf{E}_x\|^2 + c_4 \|\mathbf{E}_x\| [\ell_1 \|\mathbf{E}_x\|^2 + \ell_2 \|\mathbf{E}_x\| \|\hat{\mathbf{x}}\| \\ &\quad + \ell_3 \beta_y (\|\mathbf{y}(0)\|, \tau) + \ell_3 \xi + \ell_4 \varepsilon]. \end{aligned} \quad (34)$$

For $\|\mathbf{E}_x\| \leq c_3/(2c_4\ell_1)$, using Assumption 2, it follows that

$$\begin{aligned} \dot{V}_2 &\leq -2 \left\{ c_3 - c_4 \ell_1 \left[\hat{\beta}_x (\|\hat{\mathbf{x}}(0)\|, t) + \hat{\alpha}_x (\|\mathbf{u}\|) \right] \right\} V_2 \\ &\quad + 2 [\ell_3 \varepsilon + \ell_3 \xi + \ell_4 \beta_y (\|\mathbf{y}(0)\|, \tau)] \sqrt{V_2} \\ &\leq -2 \left\{ \ell_a - \ell_b \hat{\beta}_x (\|\hat{\mathbf{x}}(0)\|, t) \right\} V_2 \\ &\quad + 2 [\ell_c \varepsilon + \ell_d \beta_y (\|\mathbf{y}(0)\|, \tau)] \sqrt{V_2}, \end{aligned} \quad (35)$$

where $0 < \ell_a \leq c_3 - c_4 \ell_1 \hat{\alpha}_x (\sup \|\mathbf{u}\|)$, $\ell_c \geq \ell_3(1 + \xi/\varepsilon) > 0$, and $\ell_b, \ell_d > 0$. Using the comparison lemma, we have

$$\begin{aligned} W_2(t) &\leq \phi(t, 0) W_2(0) \\ &\quad + \int_0^t \phi(t, s) [\ell_c \varepsilon + \ell_d \beta_y (\|\mathbf{y}(0)\|, \tau)] ds, \end{aligned} \quad (36)$$

where $W_2 = \sqrt{V_2}$ and

$$|\phi(t, s)| \leq \ell_e e^{-\ell_f t}, \quad \text{for } \ell_e, \ell_f > 0. \quad (37)$$

Because

$$\int_0^t e^{-\ell_f s} \beta_y (\|\mathbf{y}(0)\|, \tau) ds = O(\varepsilon), \quad (38)$$

it can be verified that $W_2(t) = O(\varepsilon)$. Then it follows that $\mathbf{E}_x(t, \varepsilon) = O(\varepsilon)$, and this means that (18) holds.

Since we have already verified that (22) holds in the first step, then by Assumption 3, it follows that

$$\begin{aligned} \mathbf{E}_y(t, \varepsilon) &= \|\mathbf{z}(t, \varepsilon) - \mathbf{h}(\hat{\mathbf{x}}(t, \varepsilon), \mathbf{u}(t)) - \hat{\mathbf{y}}(\tau)\| \\ &= \|\mathbf{y}(t, \varepsilon) - \hat{\mathbf{y}}(\tau)\| \leq \|\mathbf{y}(t, \varepsilon)\| + \|\hat{\mathbf{y}}(\tau)\| \\ &\leq \beta_y (\|\mathbf{y}(0)\|, \tau) + \alpha_y(\varepsilon) + \hat{\beta}_y (\|\hat{\mathbf{y}}(0)\|, \tau) = O(\varepsilon) \end{aligned} \quad (39)$$

for given initial points and all $t \geq 0$. This proves (19). According to Assumption 3, $\hat{\mathbf{y}}(\tau) = \hat{\beta}_y (\|\mathbf{y}(0)\|, \tau) \rightarrow 0$ as $\varepsilon \rightarrow 0$. Thus, the term $\hat{\mathbf{y}}(\tau) = O(\varepsilon)$ for all $t \geq T > 0$ if ε is small enough to satisfy

$$\hat{\beta}_y (\|\mathbf{y}(0)\|, \tau) \leq k\varepsilon \quad (40)$$

Let ε^{**} and T denote a solution of (40) with equal sign. Subsequently, (20) holds for all $\varepsilon \leq \varepsilon^{**}$ uniformly on $[T, \infty)$.

Finally, we prove the ISS of original slow dynamics. Since

$$\|\mathbf{x}(t, \varepsilon)\| - \|\hat{\mathbf{x}}(t)\| \leq \|\mathbf{x}(t, \varepsilon) - \hat{\mathbf{x}}(t)\| = O(\varepsilon), \quad (41)$$

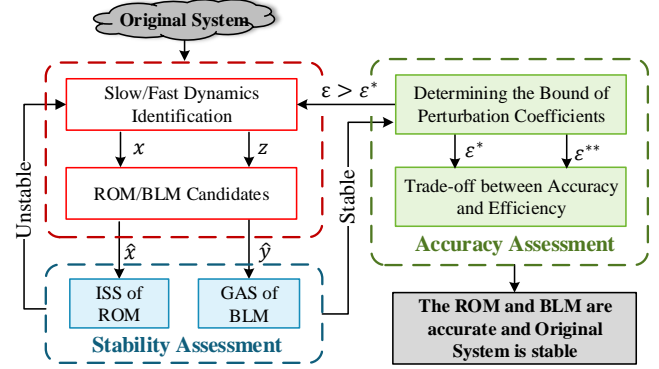


Fig. 2. The diagram of stability and accuracy assessment embedded LSOR.

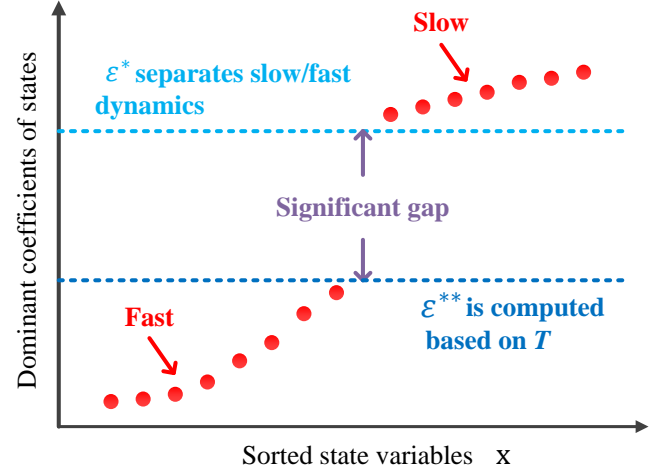


Fig. 3. Illustration of slow/fast dynamics separation by determining ε^* . The smaller value of the dominant coefficient indicates faster speed. If all the dominant coefficients of fast states are smaller than ε^{**} , the solution of BLM $\hat{\mathbf{y}}$ converges to zero within time T .

there exist some class \mathcal{KL} function β_x , class \mathcal{K} function α and a small positive constant ε_3 , such that the solution of (10a) exists for all $t \geq 0$ and $\varepsilon \leq \varepsilon^* := \min \{\varepsilon_1, \varepsilon_2, \varepsilon_3\}$ satisfying

$$\begin{aligned} \|\mathbf{x}(t, \varepsilon)\| &\leq \|\hat{\mathbf{x}}(t)\| + O(\varepsilon) \\ &\leq \hat{\beta}_x (\|\hat{\mathbf{x}}(0)\|, t) + \hat{\alpha}_x (\|\mathbf{u}\|) + O(\varepsilon) \\ &\leq \beta_x (\|\mathbf{x}(0)\|, t) + \alpha_x (\|\mathbf{u}\|) + \xi. \end{aligned} \quad (42)$$

This completes the proof of (21). \square

C. Stability and Accuracy Assessment Embedded LSOR

This subsection develops a novel LSOR method by embedding the above theorem. The overall flowchart is shown in Fig. 2 and the detailed algorithm is proposed in *Algorithm 1*.

Algorithm 1 provides a method to identify the slow and fast dynamics of a system with guaranteed stability and accuracy. The feasibility of *Algorithm 1* relies on the inherent singularly perturbed nature of inverter-based MGs, indicating the existence of at least one significant gap among the dynamic speeds of the states. To quantitatively analyze the relationship between the gap size and dynamic performance of the reduced model, we have introduced an additional threshold ε^{**} in *Algorithm 1*, whose efficacy has been proved in *Theorem 1*. The relationship between ε^* and ε^{**} is illustrated in Fig. 3. A numerical case

study is given in the next section to demonstrate how ε^{**} helps balance the accuracy and computational cost.

On the other hand, it is also possible that different partitions of fast and slow dynamics result in similar performance of the ROM. Choosing more dynamics as fast ones can reduce the order of the ROM and improve the computational efficiency, but it can also compromise the accuracy. Therefore, a careful trade-off should be made according to the engineering requirements. For instance, in the MG control problem, minimizing the computational time of solving differential equations is not a priority. In this case, as long as the computational speed meets the sampling rate requirement to avoid input time delays, it is preferable to use a higher-order but more accurate ROM to design the controller [38]. On the other hand, if the modeling error tolerance is higher while the computational burden is more critical, such as in some qualitative analysis, then it is suggested to consider more states as fast ones [26].

This algorithm is designed for MGs with two-time-scale properties, however, no basic assumptions of the MGs are required. Therefore, the proposed method can be applied to arbitrary dynamic systems.

Algorithm 1 Stability/Accuracy Assessment Embedded LSOR

```

1: Choose the smaller parameters dominating the transient
   velocity as  $\varepsilon$ . The states with respect to  $\varepsilon$  are identified
   as fast states, while the others as slow states.
2: procedure ROM AND BLM DERIVATION
3:   Let  $\varepsilon = 0$ , solve the algebraic equation (11) to obtain
   the isolated QSS solutions  $\mathbf{z} = \mathbf{h}(\mathbf{x}, \mathbf{u})$ 
4:   Substitute  $\mathbf{z}$  into (10a), obtaining the ROM (13)
5:   Derive the BLM using equation (15).
6: end procedure
7: procedure STABILITY ASSESSMENT
8:   if Assumption 2 and 3 are satisfied then
9:     Go to next procedure
10:  else
11:    Return to Step 1 to re-identify slow/fast dynamics.
12:  end if
13: end procedure
14: procedure CALCULATE THE BOUND OF  $\varepsilon$ 
15:   Calculate  $\varepsilon^* = \min\{\varepsilon_1, \varepsilon_2, \varepsilon_3\}$  according to proof.
16:   Calculate  $\varepsilon^{**}$  by solving equation (40) with equal sign.
17: end procedure
18: procedure ACCURACY ASSESSMENT
19:   if  $\varepsilon \leqslant \varepsilon^*$  then
20:     if  $\varepsilon \leqslant \varepsilon^{**}$  then
21:        $\mathbf{z} = \mathbf{h}(\hat{\mathbf{x}}, \mathbf{u})$  is the solution of fast dynamics
22:     else
23:       Use  $\mathbf{z} = \mathbf{h}(\hat{\mathbf{x}}, \mathbf{u}) + \hat{\mathbf{y}}$  by solving the BLM (15).
24:     end if
25:   else
26:     Return to Step 1 to re-identify slow/fast dynamics
27:   end if
28: end procedure
```

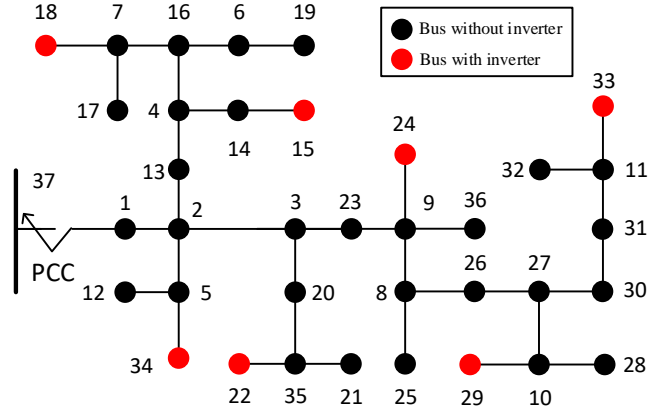


Fig. 4. The diagram of modified IEEE-37 bus system.

IV. CASE STUDY

A. Simulation Setup

The proposed method is tested on a modified IEEE-37 bus MG, which can be operated in grid-tied or islanded modes as shown in Fig. 4. According to [26], seven inverters are connected to buses 15, 18, 22, 24, 29, 33, and 34. When the point of common coupling (PCC) is closed, the MG is operated in grid-tied mode. Otherwise, it is operated in islanded mode.

We first let the MG be operated in grid-tied mode. In order to analyze the detailed dynamic properties of both slow and fast dynamics as well as compare our method with the small-signal order reduction approach, a single bus of interest (bus 34) is chosen to show its dynamic responses after power command (input) changes for clearance. Then, a simulation is conducted in islanded mode to show the dynamic responses of multiple buses with DERs when a load sudden change is given to verify its effectiveness against large disturbances. The detailed load and line parameter settings can be found in [26].

B. Performance in Grid-tied Mode and Comparison With Small-Signal ROM

We start by defining a set of candidate coefficients that dominate the dynamic response speeds to identify the slow and fast dynamics. In [26], [27], the dominant coefficients are selected as the common coefficients of the state variables and their derivative terms. This selection has been verified within a neighborhood of an equilibrium using modal analysis and tested with hardware experiments in [27]. However, this method may not be applicable to nonlinear systems in our problem. For nonlinear systems, there is no general method like spectral analysis in linear systems that can precisely measure the dynamic response speeds.

To overcome this challenge, we first approximately follow the definition of dominant coefficients which has been validated on a small-signal model of the MG in [27]. Then, we select the smaller coefficients as perturbation coefficients ε . Finally, if the derived ROM and BLM pass the proposed stability and accuracy assessment in Theorem 1, this candidate ε and the corresponding separation of slow and fast dynamics are theoretically verified. If not, we need to re-identify the

slow and fast dynamics by lowering the threshold of ε and considering different combinations of parameters as dominant coefficients in the differential equations.

Considering the MG model in grid-tied mode, the derivative term can be rewritten as

$$\left(\begin{array}{l} \frac{1}{\omega_c} \dot{P}_i, \frac{1}{\omega_c} \dot{Q}_i, \dot{\Phi}_{\text{PLL}i}, \dot{\delta}_i, \frac{K_{\text{P},Pi}}{K_{\text{I},Pi}} \dot{\Phi}_{\text{Pi}}, \frac{K_{\text{P},Pi}}{K_{\text{I},Pi}} \dot{\Phi}_{\text{Qi}}, \\ \frac{K_{\text{P},Ci}}{K_{\text{I},Ci}} \dot{\Gamma}_{di}, \frac{K_{\text{P},Ci}}{K_{\text{I},Ci}} \dot{\Gamma}_{qi}, \frac{1}{\omega_{c,\text{PLL}i}} \dot{V}_{od,fi}, \frac{L_{fi}}{R_{fi}} \dot{I}_{ldi}, \\ \frac{L_{fi}}{R_{fi}} \dot{I}_{lqi}, \frac{L_{ci}}{R_{ci}} \dot{I}_{odi}, \frac{L_{ci}}{R_{ci}} \dot{I}_{oqi}, \frac{C_{fi}}{R_{di}} \dot{V}_{odi}, \frac{C_{fi}}{R_{di}} \dot{V}_{oqi} \end{array} \right) \quad (43)$$

Substituting the parameters in [39] into the vector (43), we have

$$\begin{aligned} & \left(\begin{array}{l} \frac{1}{50.26} \dot{P}_i, \frac{1}{50.26} \dot{Q}_i, \dot{\Phi}_{\text{PLL}i}, \dot{\delta}_i, \frac{0.5}{25} \dot{\Phi}_{di}, \frac{0.5}{25} \dot{\Phi}_{qi}, \frac{1}{100} \dot{\Gamma}_{di}, \\ \frac{1}{100} \dot{\Gamma}_{qi}, \frac{1}{7853.98} \dot{V}_{od,fi}, \frac{0.0042}{0.5} \dot{I}_{ldi}, \frac{0.0042}{0.5} \dot{I}_{lqi}, \\ \frac{0.0005}{0.09} \dot{I}_{odi}, \frac{0.0005}{0.09} \dot{I}_{oqi}, \frac{0.000015}{2.025} \dot{V}_{odi}, \frac{0.000015}{2.025} \dot{V}_{oqi} \end{array} \right) \\ & = \left(\begin{array}{l} 0.02 \dot{P}_i, 0.02 \dot{Q}_i, \dot{\Phi}_{\text{PLL}i}, \dot{\delta}_i, 0.02 \dot{\Phi}_{di}, 0.02 \dot{\Phi}_{qi}, 0.01 \dot{\Gamma}_{di}, \\ 0.01 \dot{\Gamma}_{qi}, 1.3 \times 10^{-4} \dot{V}_{od,fi}, 8.4 \times 10^{-3} \dot{I}_{ldi}, 8.4 \times 10^{-3} \dot{I}_{lqi}, \\ 1.4 \times 10^{-3} \dot{I}_{odi}, 1.4 \times 10^{-3} \dot{I}_{oqi}, 7.4 \times 10^{-6} \dot{V}_{odi}, 7.4 \times 10^{-6} \dot{V}_{oqi} \end{array} \right). \end{aligned}$$

It can be seen that the magnitudes of dominant coefficients vary significantly, which is caused by the two-time-scale property of the system. The smaller parameters are selected as perturbation coefficients ε , which are utilized to classify the slow and fast states in this system:

$$\mathbf{x}_1 = [P_i \ Q_i \ \Phi_{\text{PLL}i} \ \delta_i \ \Phi_{\text{Pi}} \ \Phi_{\text{Qi}} \ \Gamma_{di} \ \Gamma_{qi}]^\top, \quad (44)$$

$$\mathbf{z}_1 = [V_{odfi} \ I_{ldi} \ I_{lqi} \ I_{odi} \ I_{oqi} \ V_{odi} \ V_{oqi}]^\top. \quad (45)$$

Remark 4: The concepts of slow and fast dynamics are relative and depend on the specific parameter settings. Different parameters can alter the dynamic response speeds of the states accordingly. For instance, the states associated with PI controllers are regarded as slow dynamics under the parameter setting in [39], but as fast dynamics under the parameter setting in [26]. Hence, the identification of slow and fast dynamics should take into account the detailed parameter setting, and the results (44)-(45) are not generalizable for any MGs.

We first set ε to 0 and calculate the QSS solution $\mathbf{z}_1 = \mathbf{h}(\mathbf{x}_1, \mathbf{u}_1)$ by solving the algebraic equation with respect to the fast dynamics (45). Then the ROM is obtained by substituting \mathbf{z}_1 into the slow dynamic equations with respect to (44). Comparing the numbers of state variables in equation (43) and (44), the order of the original model is reduced to 53.33%. Then we derive the BLM using equation (15). Once the ROM and BLM are obtained, we use the conventional ISS and GAS judging theorems in [21] to evaluate their stability of them. Specially, the unforced nonlinear ROM is exponentially stable by checking that its linearized system matrix has eigenvalues with strictly negative real parts. It can be verified that the assumptions are satisfied. Based on this result, we are inclined to anticipate the stability of the original system.

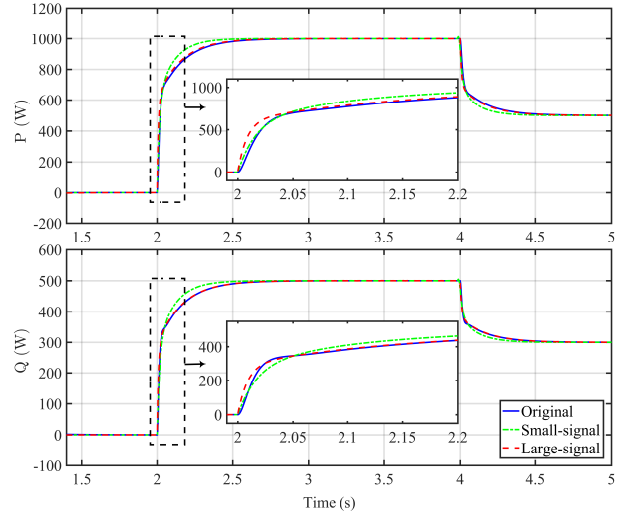


Fig. 5. Simulation results of slow and fast dynamic responses of interested bus 34: active and reactive power.

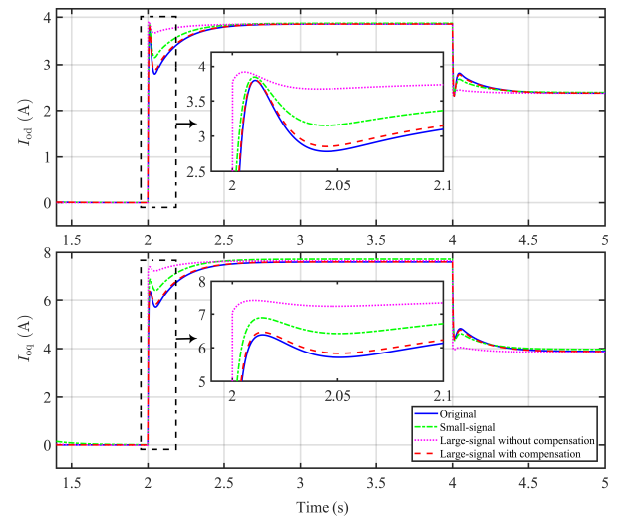


Fig. 6. Simulation results of slow and fast dynamic responses of interested bus 34: dq -axis output currents I_{od} and I_{oq} .

To ensure this, we still need to theoretically verify the accuracy of the ROM and BLM. Following the technique in the proof, we can calculate the boundary of ε as $\varepsilon^* = \min\{\varepsilon_1, \varepsilon_2, \varepsilon_3\} = 7.92 \times 10^{-3}$. Note that $\max\{\varepsilon\} = 3.9 \times 10^{-3} < 7.92 \times 10^{-3} = \varepsilon^*$. Therefore, we can conclude that this MGs system is stable and we can use the solutions of its ROM $\dot{\mathbf{x}}$ and $\mathbf{z} = \mathbf{h}(\dot{\mathbf{x}}, \mathbf{u}) + \dot{\mathbf{y}}$ to accurately represent its real dynamic responses. Furthermore, given $T = 0.43$ s, we can find a ε^{**} satisfying $\max\{\varepsilon\} < \varepsilon^{**} = 4.2 \times 10^{-3}$, which indicates that the term $\dot{\mathbf{y}}$ will be $O(\varepsilon)$ after 0.43 s. Here, a trade-off exists between accuracy and efficiency. When the accuracy is prior, one can choose $\mathbf{z} = \mathbf{h}(\dot{\mathbf{x}}, \mathbf{u}) + \dot{\mathbf{y}}$ by computing an additional differential equation (BLM). When the efficiency dominates, use $\mathbf{z} = \mathbf{h}(\dot{\mathbf{x}}, \mathbf{u})$ suffering the inaccuracy only within $(0, T)$.

Then we conduct the simulation of the derived ROM using MATLAB. The active power command changes to 1000 W at 2 s and changes to 500 W at 4 s. The reactive power

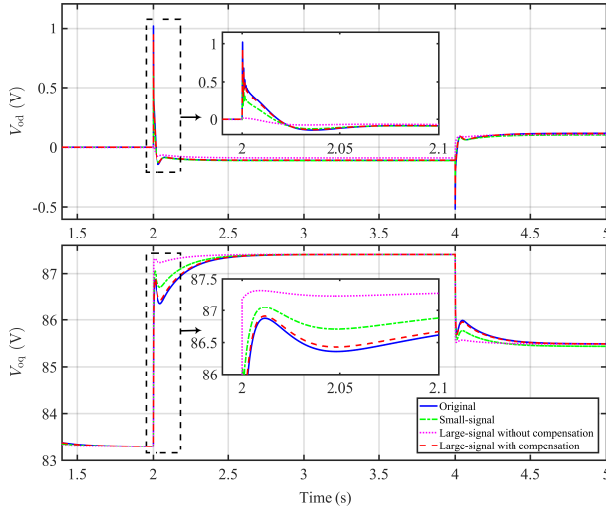


Fig. 7. Simulation results of slow and fast dynamic responses of interested bus 34: dq -axis output voltages V_{od} and V_{oq} .

command changes to 500 W at 2 s and changes to 300 W at 4 s. A comparison simulation using the small-signal order reduction method in [27] is conducted under the same conditions. The simulation results are shown in Fig. 5-7, where blue solid lines denote the responses of the original model, green dash-dotted lines denote that using small-signal order reduction method, pink dotted lines denote the results of proposed LSOR without BLM compensation (i.e., QSS solution), and red dashed lines are the responses with the addition of solution \hat{y} of BLM (i.e. $z = h + \hat{y}$). For the main slow dynamics (active and reactive powers) shown in (a), the proposed LSOR method is more accurate than the small-signal model during the transient period. Regarding the fast dynamics voltages and currents illustrated in (b) and (c), the LSOR method with compensation \hat{y} provides the most accurate performance. However, the LSOR without \hat{y} gives worse performance than the small-signal one used in [27]. This is because the fast dynamics predicted by the method in [27] are also compensated with a corrected response. From the stability point of view, the red lines in Fig. 5-7 show that, with bounded input power commands, both ROM and BLM are stable, which indicates that the original system is stable as justified by the stability of blue lines. To systematically evaluate the quantitative contrasts in the dynamic behaviors of both the proposed large-signal and small-signal order reduction methods, we present the root-mean-square errors (RMSEs) computed from the results displayed in Figs. 5-7. As tabulated in Table I, these RMSE values are sufficiently small when compared to the magnitudes of their corresponding state variables. It is important to note that the compensation facilitated by the BLM exclusively pertains to fast dynamics. Thus, the respective cells of active/reactive powers which are identified as slow dynamics in this case in Table I remain unpopulated.

C. Computational Efficiency Analysis

In order to evaluate the computational efficiency of the pro-

TABLE I
RMSES OF SLOW AND FAST DYNAMICS USING LSOR, LSOR WITH BLM COMPENSATION, AND SMALL-SIGNAL ORDER REDUCTION METHODS.

| Model State \ Model State | LSOR | LSOR w/ compensation | Small-signal |
|---------------------------|-------|----------------------|--------------|
| P (kW) | 0.014 | | 0.019 |
| Q (kVAR) | 0.004 | | 0.008 |
| I_{od} (A) | 0.257 | 0.021 | 0.101 |
| I_{oq} (A) | 0.499 | 0.040 | 0.227 |
| V_{od} (V) | 0.022 | 0.002 | 0.008 |
| V_{oq} (V) | 0.286 | 0.023 | 0.127 |

TABLE II
COMPUTATIONAL TIME OF ORIGINAL, SMALL-SIGNAL AND LARGE-SIGNAL ROMS USING DIFFERENT ODE SOLVERS.

| Model Solver \ Model Solver | Original model | Large-signal | Small-signal |
|-----------------------------|----------------|--------------|--------------|
| ode45 | 94.25 s | 11.92 s | 9.56 s |
| ode15s | 11.43 s | 10.81 s | 8.24 s |

posed SPT-based method, particularly from the viewpoint of reducing stiffness, two different ordinary differential equation (ODE) solvers are implemented: ode45 solver and ode15s solver. Stiffness is a property of a system of ordinary differential equations that affects the numerical stability and efficiency of solving the system. A system is stiff if it has some components that vary much faster than others, or if it has some solutions that decay much faster than the solution of interest [40]. In such cases, a nonstiff numerical method, such as ode45 in MATLAB, would require very small time steps to capture the rapid changes or avoid numerical oscillations, which would result in a large computational cost and possibly loss of accuracy. A stiff numerical method such as ode15s in MATLAB, on the other hand, can handle larger time steps and maintain stability and accuracy. However, it may slightly reduce the accuracy of the solution.

Table II demonstrates that the ode45 solver achieves a more significant reduction in computational time than the ode15s solver when applied to the reduced-order models obtained from the original full-order model. This comparison suggests that our LSOR method transforms the original model from a *stiff* ODE problem to a *non-stiff* one. The proposed method also enhances the stability of the ODE-solving process through this transformation. Therefore, the proposed method can decrease the computational time from two aspects: the order of the system and the stiffness of the ODE problem. Furthermore, the small-signal order reduction method is slightly faster than the LSOR method. This is because the LSOR results in a set of ODEs with many nonlinear terms, which require more time to solve than a linear one. However, as Table I indicates, the accuracy of the small-signal method is lower than the proposed LSOR method.

Remark 5: Note that with the addition of the solution of BLM, we need to solve another set of differential equations. This seems that the proposed method has limited ability to

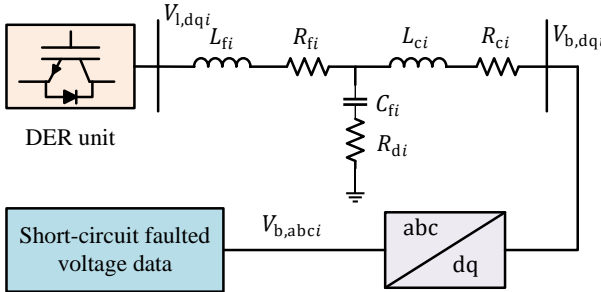


Fig. 8. Diagram illustrating the implementation of short-circuit fault test.

reduce the computational burden. However, this is not the case. As discussed above, SPT reduces the computational burden not only by reducing the number of differential equations but also by converting the *stiff* problem to a *non-stiff* one. Moreover, the adopted example is a possible worst case that the perturbation coefficients are not small enough. When ε is sufficiently small, the converging time T can be sufficiently small as well. Then we can directly use the algebraic equation to estimate the fast states.

D. Performance in Grid-tied Mode under Short-Circuit Faults

In the preceding subsections, we examined the performance of our proposed LSOR method under external disturbances induced by load sudden changes. To gain deeper theoretical insights, we investigated how load sudden changes influence the inverters' internal states through the power controller (5). Seeking a comprehensive understanding of various external disturbances' influence on the dynamic performance of the ROM, we further explore the impact of disturbance induced by short-circuit faults in this subsection. In contrast to load sudden changes, the influence of short-circuit faults is transmitted through the bus voltages V_{bd} and V_{bq} connected to the LC filter of the DER, as detailed in (9). This discovery establishes a theoretical foundation that streamlines the simulation setup. Illustrated in Fig. 8, this approach allows us to concentrate

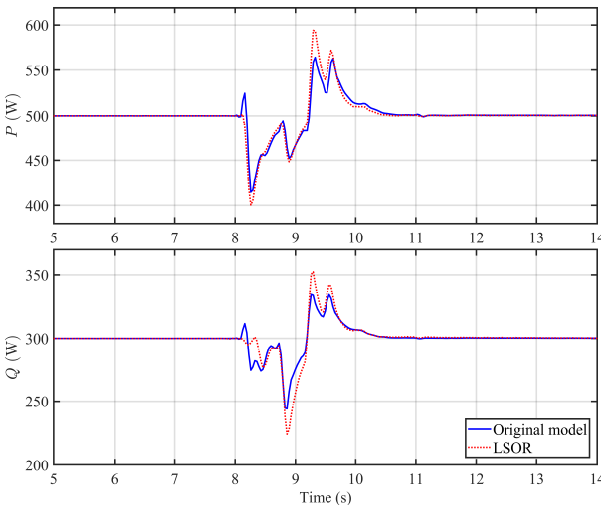


Fig. 9. Simulation results of slow and fast dynamic responses of the interested bus 34 under short-circuit fault disturbance: active and reactive power.

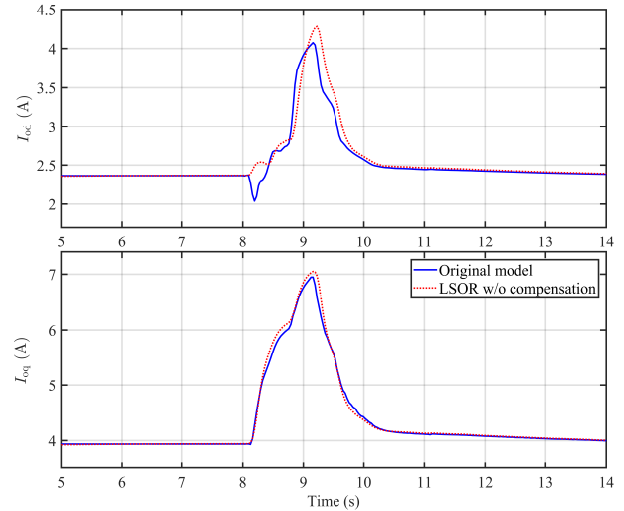


Fig. 10. Simulation results of slow and fast dynamic responses of the interested bus 34 under short-circuit fault disturbance: dq -axis output currents I_{od} and I_{oq} .

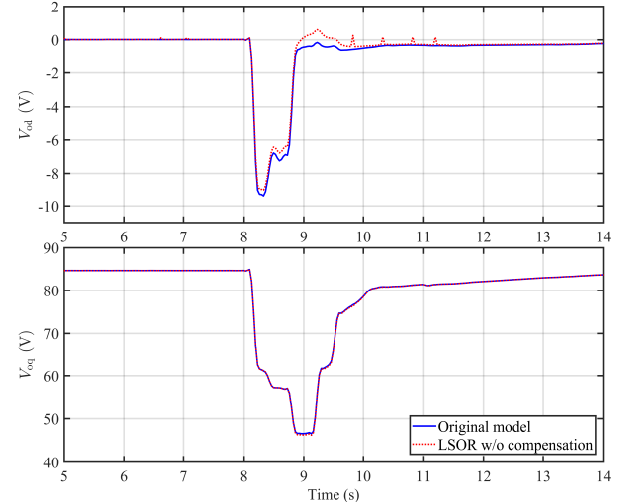


Fig. 11. Simulation results of slow and fast dynamic responses of the interested bus 34 under short-circuit fault disturbance: dq -axis output voltages V_{od} and V_{oq} .

on the key variables influencing order reduction performance, ensuring efficiency in our simulation.

The fault scenario replicates real-world conditions by adopting time-varying real utility-measured faulted voltage data. The fault sequence stages short-circuit scenarios, starting with an A-B fault at 5 seconds, followed by an A-B-G fault at 5.24 seconds, and a more severe three-phase fault at 5.63 seconds. The sequence concludes with fault clearance at 6.38 seconds, restoring the system to its normal operating state. Same as in Section IV.B, the DER at the interested bus 34 is analyzed.

Figs. 9-11 compare the dynamic responses of the proposed SPT-based LSOR and the original full-order model for the states $(P, Q, I_{od}, I_{oq}, V_{od}, V_{oq})$, which have RMSEs of $(0.01, 0.01, 0.01, 0.01, 0.01, 0.01)$. The results show that the proposed SPT-based LSOR method can accurately capture both the slow and fast dynamics of the original full-order model under the complex short-circuit fault scenario, which

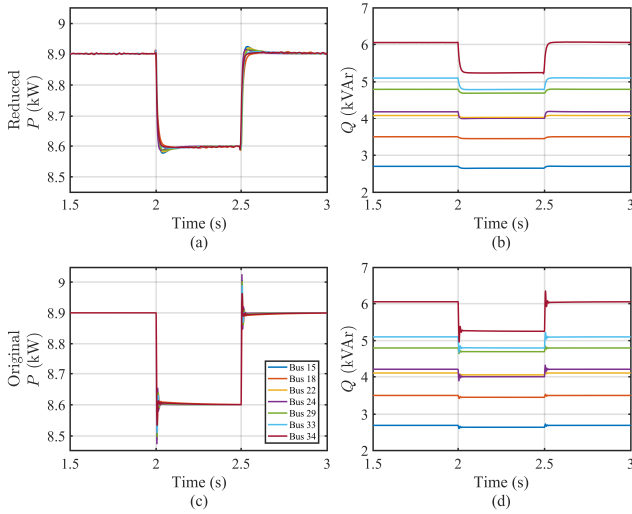


Fig. 12. Comparison of the active/reactive power of the seven buses with DERs of original and reduced systems: (a)-(b) denote the responses of the reduced-order system, (c)-(d) are the responses of the original system.

demonstrates its effectiveness and robustness.

E. Performance in Islanded Mode under Load Sudden Change

In this subsection, a simulation in islanded mode is conducted to verify the effectiveness of the proposed method by showing the dynamic responses of the buses with DERs. To study the dynamic characteristics, a $20\ \Omega$ load is connected parallel to bus 12 at 2 s and disconnected at 2.5 s. Following the similar procedure in case 1, we can identify the slow and fast dynamics of this multi-bus system. Despite the different parameter settings of inverters, the relative magnitudes of derivative terms' coefficients still hold uniformly. That means we can obtain a uniform division of slow and fast dynamics. This fact is based on the nature of different components' time scales. The slow and fast states are divided as follows,

$$\mathbf{x}_2 = [P_i \ Q_i \ \Phi_{PLL_i} \ \delta_i \ \Phi_{di} \ \Gamma_{qi} \ \Gamma_{di} \ \Gamma_{qi}]^\top, \quad (46)$$

$$\mathbf{z}_2 = [V_{odfi} \ I_{ldi} \ I_{lqi} \ I_{odi} \ I_{oqi} \ V_{odi} \ V_{oqi}]^\top. \quad (47)$$

TABLE III

COMPUTATIONAL TIME OF ORIGINAL AND REDUCED-ORDER MODELS USING DIFFERENT ODE SOLVERS IN ISLANDED MODE.

| Model Solver | Original model | Reduced model | Percentage |
|-----------------|----------------|---------------|------------|
| ode45 | 104.25 s | 11.25 s | 89.2% |
| ode15s | 13.23 s | 11.37 s | 14% |

The ROM can be derived using the *Algorithm 1*. The order of the original model is reduced from 105th to 56th. The simulation time is shown in Table III. Same as analyzed in the last case study, the proposed method can convert the stiff model of islanded MG to a non-stiff one to reduce the computational burden. Figs. 12-14 show the dynamic responses of the original and reduced models of seven buses with DERs. The comparison between the results of the original

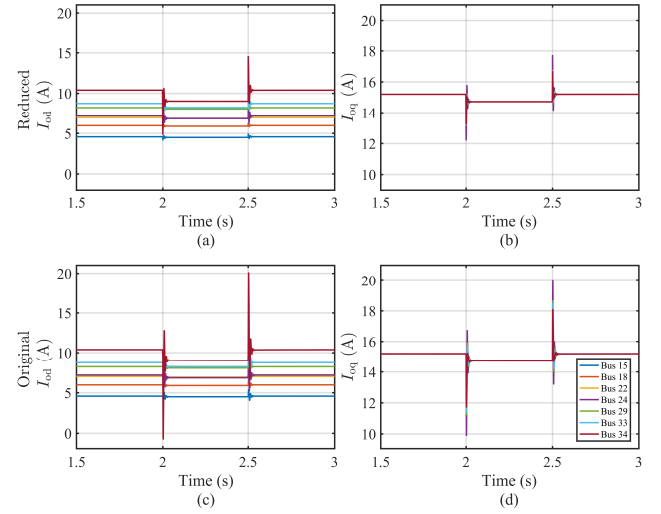


Fig. 13. Comparison of the dq -axis output currents of the seven buses with DERs of original and reduced systems: (a)-(b) denote the responses of the reduced-order system, (c)-(d) are the responses of the original system.

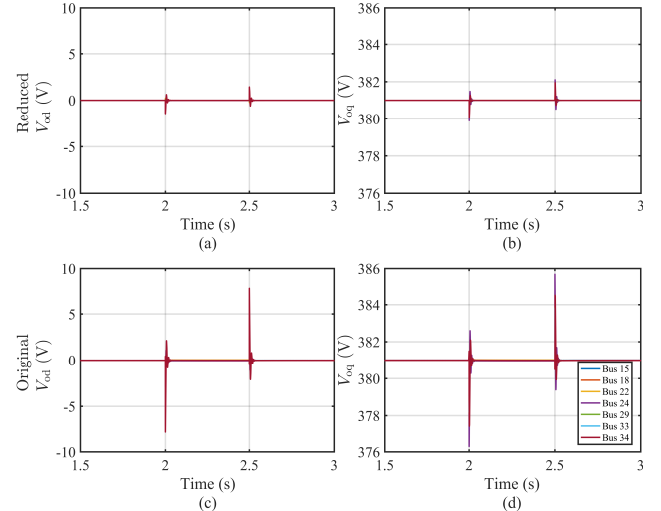


Fig. 14. Comparison of the dq -axis output voltages of the seven buses with DERs of original and reduced systems: (a)-(b) denote the responses of the reduced-order system, (c)-(d) are the responses of the original system.

model and the reduced one shows the accuracy of the ROM. In addition, the responses under load sudden change verify the effectiveness of our method against large disturbances in islanded systems.

V. CONCLUSION

This paper proposes an LSOR approach for MGs in the EMT time scale with consideration of external control input by synthesizing a novel stability and accuracy assessment theorem. The advantages of our proposed theorem can be summarized into two aspects. Firstly, one can determine the stability of a full-order system by only analyzing the stability of its derived ROM and BLM. Specially, when the ROM is input-to-state stable and the BLM is uniformly globally asymptotically stable, the original MG system can be proved to be stable under several common growth conditions. This

makes it easier and more feasible to determine the stability of a high-order system. Secondly, a set of quantitative accuracy assessment criteria is developed and embedded into a tailored feedback mechanism to guarantee the accuracy of the derived ROM. It is proved that the errors between solutions of reduced and original models are bounded and convergent under such conditions. The above stability and accuracy theorem has been strictly proven indicating that the proposed method is generic for arbitrary dynamic systems satisfying the given assumptions. Finally, we have conducted multiple simulations under different conditions on an IEEE standard MG system to verify the effectiveness of the proposed method.

The suggested LSOR method holds promise for future extensions. One potential avenue involves exploring its applicability across diverse classes of nonlinear systems, encompassing uncertainties, time-varying coefficients, time delays, and similar complexities. Investigating whether the established sufficient conditions for stability and accuracy of ROM can be extended to these intricate systems would be a valuable pursuit. Another potential extension lies in integrating the proposed LSOR method with nonlinear control and optimization techniques. This could involve designing stabilizing controllers based on the ROM for high-order systems, presenting an opportunity to streamline the complexity of controller design.

REFERENCES

- [1] M. Shahidehpour and J. F. Clair, "A functional microgrid for enhancing reliability, sustainability, and energy efficiency," *Electr. J.*, vol. 25, no. 8, pp. 21 – 28, Oct. 2012.
- [2] C. Wang, B. Cui, and Z. Wang, "Analysis of solvability boundary for droop-controlled microgrids," *IEEE Trans. Power Syst.*, vol. 33, no. 5, pp. 5799–5802, Sep. 2018.
- [3] C. Wang, P. Ju, S. Lei, Z. Wang, F. Wu, and Y. Hou, "Markov decision process-based resilience enhancement for distribution systems: An approximate dynamic programming approach," *IEEE Trans. Smart Grid*, vol. 11, no. 3, pp. 2498–2510, May 2020.
- [4] Z. Ma, Z. Wang, Y. Guo, Y. Yuan, and H. Chen, "Nonlinear multiple models adaptive secondary voltage control of microgrids," *IEEE Trans. Smart Grid*, vol. 12, no. 1, pp. 227–238, Jan. 2021.
- [5] Q. Zhang, Z. Ma, Y. Zhu, and Z. Wang, "A two-level simulation-assisted sequential distribution system restoration model with frequency dynamics constraints," *IEEE Trans. Smart Grid*, vol. 12, no. 5, pp. 3835–3846, Sep. 2021.
- [6] Z. Ma, Z. Wang, and R. Cheng, "Analytical large-signal modeling of inverter-based microgrids with koopman operator theory for autonomous control," *IEEE Trans. Smart Grid*, 2023, early access. doi=10.1109/TSG.2023.3314749.
- [7] Z. Wang, B. Chen, J. Wang, J. Kim, and M. M. Begovic, "Robust optimization based optimal dg placement in microgrids," *IEEE Trans. Smart Grid*, vol. 5, no. 5, pp. 2173–2182, Sep. 2014.
- [8] X. Lu, K. Sun, J. M. Guerrero, J. C. Vasquez, L. Huang, and J. Wang, "Stability enhancement based on virtual impedance for DC microgrids with constant power loads," *IEEE Trans. Smart Grid*, vol. 6, no. 6, pp. 2770–2783, Nov. 2015.
- [9] Z. Ma, Q. Zhang, and Z. Wang, "Safe and stable secondary voltage control of microgrids based on explicit neural networks," *IEEE Trans. Smart Grid*, vol. 14, no. 5, pp. 3375–3387, Sep. 2023.
- [10] Y. Li, P. Zhang, L. Zhang, and B. Wang, "Active synchronous detection of deception attacks in microgrid control systems," *IEEE Trans. Smart Grid*, vol. 8, no. 1, pp. 373–375, Jan. 2017.
- [11] C. Wang, Y. Hou, F. Qiu, S. Lei, and K. Liu, "Resilience enhancement with sequentially proactive operation strategies," *IEEE Trans. Power Syst.*, vol. 32, no. 4, pp. 2847–2857, Jul. 2017.
- [12] Y. Li, P. Zhang, and M. Yue, "Networked microgrid stability through distributed formal analysis," *Appl. Energy*, vol. 228, pp. 279 – 288, Oct. 2018.
- [13] Z. Li and M. Shahidehpour, "Small-signal modeling and stability analysis of hybrid AC/DC microgrids," *IEEE Trans. Smart Grid*, vol. 10, no. 2, pp. 2080–2095, Mar. 2019.
- [14] J. Fu, Z. Ma, Y. Fu, and T. Chai, "Hybrid adaptive control of nonlinear systems with non-Lipschitz nonlinearities," *Systems & Control Letters*, vol. 156, p. 105012, Oct. 2021.
- [15] Y. Wang, Z. Yi, D. Shi, Z. Yu, B. Huang, and Z. Wang, "Optimal distributed energy resources sizing for commercial building hybrid microgrids," in *Proc. IEEE Power Energy Society General Meeting (PESGM)*, Aug. 2018, pp. 1–5.
- [16] N. Herath and D. Del Vecchio, "Deterministic-like model reduction for a class of multiscale stochastic differential equations with application to biomolecular systems," *IEEE Trans. Autom. Control*, vol. 64, no. 1, pp. 351–358, Jan. 2018.
- [17] V. Purba, B. B. Johnson, M. Rodriguez, S. Jafarpour, F. Bullo, and S. V. Dhople, "Reduced-order aggregate model for parallel-connected single-phase inverters," *IEEE Trans. Energy Convers.*, vol. 34, no. 2, pp. 824–837, Jun. 2019.
- [18] Z. Shuai, Y. Peng, X. Liu, Z. Li, J. M. Guerrero, and Z. J. Shen, "Dynamic equivalent modeling for multi-microgrid based on structure preservation method," *IEEE Trans. Smart Grid*, vol. 10, no. 4, pp. 3929–3942, Jul. 2019.
- [19] A. Floriduz, M. Tucci, S. Riverso, and G. Ferrari-Trecate, "Approximate kton reduction methods for electrical networks with applications to plug-and-play control of ac islanded microgrids," *IEEE Trans. Control Syst. Technol.*, vol. 27, no. 6, pp. 2403–2416, Nov. 2019.
- [20] R. Wang, Q. Sun, P. Tu, J. Xiao, Y. Gui, and P. Wang, "Reduced-order aggregate model for large-scale converters with inhomogeneous initial conditions in DC microgrids," *IEEE Trans. Energy Convers.*, vol. 36, no. 3, pp. 2473–2484, Sep. 2021.
- [21] H. K. Khalil, *Nonlinear Systems*. New Jersey: Prentice Hall, 2000.
- [22] Y. Ma, D. Zhu, Z. Zhang, X. Zou, J. Hu, and Y. Kang, "Modeling and transient stability analysis for type-3 wind turbines using singular perturbation and lyapunov methods," *IEEE Trans. Ind. Electron.*, vol. 70, no. 8, pp. 8075–8086, Oct. 2023.
- [23] O. Ajala, N. Baeckeland, B. Johnson, S. Dhople, and A. Domínguez-García, "Model reduction and dynamic aggregation of grid-forming inverter networks," *IEEE Trans. Power Syst.*, 2022, early access. doi=10.1109/TPWRS.2022.3229970.
- [24] O. Ajala, M. Lu, B. Johnson, S. V. Dhople, and A. Domínguez-García, "Model reduction for inverters with current limiting and dispatchable virtual oscillator control," *IEEE Trans. Energy Convers.*, vol. 37, no. 4, pp. 2250–2259, Dec. 2022.
- [25] P. Li, L. Wang, B. Zhong, and M. Zhang, "Linear active disturbance rejection control for two-mass systems via singular perturbation approach," *IEEE Trans. Ind. Inform.*, vol. 18, no. 5, pp. 3022–3032, May 2022.
- [26] L. Luo and S. V. Dhople, "Spatiotemporal model reduction of inverter-based islanded microgrids," *IEEE Trans. Energy Convers.*, vol. 29, no. 4, pp. 823–832, Dec. 2014.
- [27] M. Rasheduzzaman, J. A. Mueller, and J. W. Kimball, "Reduced-order small-signal model of microgrid systems," *IEEE Trans. Sustain. Energy*, vol. 6, no. 4, pp. 1292–1305, Oct. 2015.
- [28] P. Vorobev, P.-H. Huang, M. Al Hosani, J. L. Kirtley, and K. Turitsyn, "High-fidelity model order reduction for microgrids stability assessment," *IEEE Trans. Power Syst.*, vol. 33, no. 1, pp. 874–887, Jan. 2017.
- [29] Z. Zhao, J. Wu, X. Luo, J. Xie, Q. Yang, Q. Ni, and L. L. Lai, "Reduced-order model for wind-solar multi-microgrids considering time-scale coupling," *IEEE Trans. Power Syst.*, pp. 1–13, 2023, early access. doi=10.1109/TPWRS.2023.3270366.
- [30] S. Anand and B. G. Fernandes, "Reduced-order model and stability analysis of low-voltage DC microgrid," *IEEE Trans. Ind. Electron.*, vol. 60, no. 11, pp. 5040–5049, Nov. 2013.
- [31] M. Kabalan, P. Singh, and D. Niebur, "Nonlinear Lyapunov stability analysis of seven models of a dc/ac droop controlled inverter connected to an infinite bus," *IEEE Trans. Smart Grid*, vol. 10, no. 1, pp. 772–781, Jan. 2019.
- [32] J. W. Simpson-Porco, F. Dörfler, F. Bullo, Q. Shafiee, and J. M. Guerrero, "Stability, power sharing, distributed secondary control in droop-controlled microgrids," in *Proc. IEEE Int. Conf. Smart Grid Communications (SmartGridComm)*, Oct. 2013, pp. 672–677.
- [33] S. Eberlein and K. Rudion, "Impact of inner control loops on small-signal stability and model-order reduction of grid-forming converters," *IEEE Trans. Smart Grid*, vol. 14, no. 4, pp. 2812–2824, Nov. 2023.
- [34] V. Mariani, F. Vasca, J. C. Vásquez, and J. M. Guerrero, "Model order reductions for stability analysis of islanded microgrids with droop control," *IEEE Trans. Ind. Electron.*, vol. 62, no. 7, pp. 4344–4354, Jul. 2015.

- [35] I. P. Nikolakakos, H. H. Zeineldin, M. S. El-Moursi, and J. L. Kirtley, "Reduced-order model for inter-inverter oscillations in islanded droop-controlled microgrids," *IEEE Trans. Smart Grid*, vol. 9, no. 5, pp. 4953–4963, Sep. 2018.
- [36] P. D. Christofides and A. R. Teel, "Singular perturbations and input-to-state stability," *IEEE Trans. Autom. Control*, vol. 41, no. 11, pp. 1645–1650, Nov. 1996.
- [37] Z. Ma, Z. Wang, D. Zhao, and B. Cui, "High-fidelity large-signal order reduction approach for composite load model," *IET Gener. Transm. Distrib.*, vol. 14, no. 21, pp. 4888–4897, Sep. 2020.
- [38] R. Mallik, B. Majmunović, S. Dutta, G.-S. Seo, D. Maksimović, and B. Johnson, "Control design of series-connected PV-powered grid-forming converters via singular perturbation," *IEEE Trans. Power Electron.*, vol. 38, no. 4, pp. 4306–4322, Nov. 2023.
- [39] M. Rasheduzzaman, J. A. Mueller, and J. W. Kimball, "An accurate small-signal model of inverter-dominated islanded microgrids using dq reference frame," *IEEE J. Emerg. Sel. Top. Power Electron.*, vol. 2, no. 4, pp. 1070–1080, Jul. 2014.
- [40] G. Söderlind, L. Jay, and M. Calvo, "Stiffness 1952–2012: Sixty years in search of a definition," *BIT Numer. Math.*, vol. 55, no. 2, pp. 531–558, Jun. 2015.



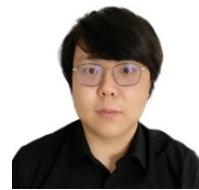
Zixiao Ma (Member, IEEE) received his B.S. degree in automation and M.S. degree in control theory and control engineering from Northeastern University, Shenyang, China, in 2014 and 2017, respectively, and the Ph.D. degree in electrical and computer engineering from Iowa State University, Ames, IA, USA, in 2023. He is currently a postdoctoral scholar in the Clean Energy Institute and Department of Electrical and Computer Engineering at the University of Washington, Seattle, WA, USA. He was the recipient of the Outstanding Reviewer Award from

IEEE Transactions on Power Systems, the Research Excellence Award from Iowa State University, the Chinese Government Award for Outstanding Self-financed Students Abroad, and the Distinguished Postdoctoral Fellowship from the University of Washington. His research interests focus on control theory and machine learning with their applications to inverter-based resources, microgrids, and load modeling.



Zhaoyu Wang (Senior Member, IEEE) received the B.S. and M.S. degrees in electrical engineering from Shanghai Jiao Tong University, and the M.S. and Ph.D. degrees in electrical and computer engineering from Georgia Institute of Technology. He is the Northrop Grumman Endowed Associate Professor with Iowa State University. His research interests include optimization and data analytics in power distribution systems and microgrids. He was the recipient of the National Science Foundation CAREER Award, the Society-Level Outstanding Young

Engineer Award from IEEE Power and Energy Society (PES), the Northrop Grumman Endowment, College of Engineering's Early Achievement in Research Award, and the Harpole-Pentair Young Faculty Award Endowment. He is the Principal Investigator for a multitude of projects funded by the National Science Foundation, the Department of Energy, National Laboratories, PSERC, and Iowa Economic Development Authority. He is the Technical Committee Program Chair (TCPC) of IEEE Power System Operation, Planning and Economics (PSOE) Committee, the Chair of IEEE PSOE Award Subcommittee, the Vice Chair of IEEE Distribution System Operation and Planning Subcommittee, and the Vice Chair of IEEE Task Force on Advances in Natural Disaster Mitigation Methods. He is an Associate Editor of IEEE TRANSACTIONS ON SUSTAINABLE ENERGY, IEEE OPEN ACCESS JOURNAL OF POWER AND ENERGY, IEEE POWER ENGINEERING LETTERS, and IET Smart Grid. He was an Associate Editor for IEEE TRANSACTIONS ON POWER SYSTEMS and IEEE TRANSACTIONS ON SMART GRID.



Yuxuan Yuan (Member, IEEE) received the B.S. and Ph.D. degree in Electrical & Computer Engineering from Iowa State University, Ames, IA, in 2017 and 2022. He is currently a Data Analysis Engineer with Electric Power Engineers. Yuxuan has extensive experience in power distribution systems specializing in smart meter data analysis, event identification and localization, customer behavior modeling, load forecasting, renewable energy integration, and distribution system state estimation using machine learning and deep learning techniques.



Tianqi Hong (Member, IEEE) received a B.Sc. degree in electrical engineering from Hohai University, China, in 2011, and an M.Sc. degree in electrical engineering from the Southeast University, China and the Engineering School of New York University in 2013. He received a Ph.D. degree from New York University in 2016. His main research interests are power system analysis, power electronics systems, microgrids, and electromagnetic design. Currently, he is an Assistant Professor at the University of Georgia. Prior to this, he was a Principal Energy

System Scientist at Argonne National Laboratory, responsible for renewable integration, power system, and microgrid. Dr. Hong is an active reviewer in the power engineering area, and he serves as an Editorial Board Member of International Transactions on Electrical Energy Systems, IEEE Transactions on Power Delivery, IEEE Transactions on Industry Applications, and IEEE Power Engineering Letters. He also serves as Special Activity Co-Chair of the IEEE IAS Industrial Power Converters Committee (IPCC).